Linking Boundary Layer Circulations and Surface Processes during FIFE 89. Part II: Maintenance of Secondary Circulation

MICKEY M.-K. WAI AND ERIC A. SMITH

Department of Meteorology and Supercomputer Computations Research Institute, The Florida State University, Tallahassee, Florida

(Manuscript received 10 June 1996, in final form 2 July 1996)

ABSTRACT

Land–atmosphere interactions are examined for three different synoptic situations during a 21-day period in the course of the First ISLSCP (International Satellite Land Surface Climatology Project) Field Experiment 1989 to better understand the relationship between biophysical feedback processes, boundary layer structure, and circulations in the boundary layer. The objective is to understand how the secondary circulation discussed in Part I of this paper was able to sustain itself throughout the duration of the 1989 intensive field campaign. The study is based on diagnostic analysis of measurements obtained from a network of surface meteorology and energy budget stations, augmented with high vertical resolution radiosonde measurements. Shallow convection associated with an undisturbed boundary layer situation and rainfall occurring during two different disturbed boundary layer situations—one associated with a surface trough, the other with the passage of a cold front—led to markedly different impacts on the surface layer and the boundary layer recovery timescale. In the undisturbed case, the growth of a cloud layer produced a negative feedback on the boundary layer by stabilizing the surface layer, and cutting off the turbulence transport of heat and moisture into the subcloud layer. The deficits in heat and moisture then led to cloud dissipation. During the surface trough development and cold front passage events, rainfall reaching the surface led to the collapse of the surface layer, decrease of surface and subsurface soil temperatures, depressed sensible heating, and a slow reduction and even temporary termination of evapotranspiration. After the rains subsided, the boundary layer recovery process began with vigorous evapotranspiration rates drying the upper soil layers on a timescale of 1–2 days. During this period, 55%–65% of the net surface available heating was used for evapotranspiration, whereas only 30%–35% went directly into boundary layer heating. As the near-surface soil moisture dropped, surface sensible heating became more important in influencing boundary layer energetics. The boundary layer required approximately two days to recover to its initial temperature in the case of the surface trough. After passage of the cold front, both the soil and boundary layer cooled and dried due to cold temperature advection. Evapotranspiration rates remained relatively large for about two days after the frontal passage. The boundary layer had not completely recovered by the end of the intensive data collection period after the frontal passage, so recovery time was at least a week. The analysis shows that with the exception of three days during the surface trough event, and two or three days during the frontal passage event, the surface-driven secondary circulation persisted.

1. Introduction

In recent years, land–atmosphere interactions have become an important research topic in boundary layer meteorology, numerical weather prediction, and climate dynamics (e.g., see Sellers and Dorman 1987; Dickinson 1989; Dastoor and Krishnamurti 1991; Brutsaert and Sugita 1992; Betts et al. 1993; Chen and Avissar 1994; Smith et al. 1994; Lynn et al. 1995; Zeng and Pielke 1995). The variable nature of soil moisture and vegetation cover affects boundary layer processes through biophysical feedbacks over a wide range of space and timescales from microscale boundary layer clouds to mesoscale boundary layer circulations, as well as regional rainfall. However, the relationship between biophysical feedbacks, atmospheric circulations, and rainfall over various space and time scales is not a fully understood process (Dickinson 1993; Sun and Mahrt 1994; Wallace 1994; Noilhan and LaCarrére 1995). This is largely because there are not enough accurate measurements of the surface exchange processes, available on appropriate space and time scales, needed to corroborate such relationships. Subsequently, the impact of variable patterns of soil moisture and vegetation cover on either the persistence or break up of boundary layer circulations and boundary layer cloudiness for different types of synoptic situations is rarely discussed. Analogous to a topographic barrier, where cloudiness and precipitation are not spatially mobile, secondary circulations over a heterogeneous surface may produce a consistent and distinct local climatology involving increased cloudiness and precipitation. In large-scale

Corresponding author address: Dr. Eric A. Smith, Department of Meteorology, The Florida State University, 306 Love Bldg., Tallahassee, FL 32306-4520.
E-mail: esmith@metsat.met.fsu.edu

models, these climatological signals are not captured in the prediction because grid scales exceed the scales of the perturbation circulations and because biophysical surface properties are not completely resolved.

To quantify surface–atmosphere exchanges of mass and energy and to reveal details of the salient biophysical feedback processes such as how vegetation cover gradients modulate boundary layer processes and in turn undergo reconfigurations, it is necessary to make accurate and simultaneous measurements of the surface energy budget and boundary layer. Such measurements can also provide a guidance to parameterize these surface exchange processes. The First ISLSCP (International Satellite and Surface Climatology Project) Field Experiment (FIFE) of 1987 and 1989 provides an excellent example of a land surface–atmosphere interaction experiment investigating the details of how soil moisture, vegetation state, and surface energy balance alter and respond to boundary layer circulations over various space and timescales. A later experiment that took place in 1992 in the African Sahel, the Hydrologic Atmospheric Pilot Experiment in the Sahel (HAPEX-Sahel), is another example, albeit with less emphasis on detailed measurements of boundary layer structure. Many of the important FIFE results have already been reported in a special volume of the *Journal of Geophysical Research—Atmospheres* (November 1992) or are in press in a follow-up volume in the same journal. Goutorbe et al. (1993) and Prince et al. (1995) have provided overviews and preliminary results of the HAPEX-Sahel campaign. A special issue devoted to the first scientific results from HAPEX-Sahel has been published in the *Journal of Hydrology* (1997, Vols. 188–189).

The measurements from FIFE-89 are of interest because, as shown by Desjardins et al. (1992), there was clear evidence of spatial heterogeneities in the surface properties in and around the FIFE study area during the fifth FIFE intensive field campaign (IFC 5) held from 23 July to 12 August 1989. Using surface-based meteorological and flux measurements, soil moisture measurements, aircraft measurements, satellite measurements, and synoptic charts, Smith et al. (1994, hereafter SEA94) conducted an observational study on the variability of vegetation state, soil moisture content, surface energy budget conditions, and boundary layer flows to determine if spatial heterogeneities in the vegetation cover and soil moisture could establish a surface-driven boundary layer circulation. The study showed that the rainfall distribution prior to IFC 5 had established northwest–southeast aligned soil moisture and vegetation density gradients over the study area; Figs. 2a,b from SEA94 provided Normalized Difference Vegetation index (NDVI) and thermal maps from SPOT and Landsat satellite imagery substantiating the presence of those gradients. These surface gradients were also evident in the horizontal fields of temperature, wind, and surface fluxes. Dynamical and scaling analyses showed evidence of a thermally direct secondary circulation consistent with the surface gradients exhibiting ascending motion over the relatively warmer and drier northwestern quadrant and descending motion over the cooler and moister southeastern quadrant. The variable nature of this circulation, which was mentioned in SEA94, is the topic of this paper.

This study seeks to better understand the relationship between biophysical feedbacks and boundary layer circulations as the synoptic situation changes. In particular, we are interested in estimating the rate at which the boundary layer recovers to its initial state after a rain event, which will determine when a sustained secondary circulation will return to its characteristic intensity. Boundary layer recovery is important to understand because it describes the process of how the boundary layer responds and adjusts to external forcing as well as the process that numerical weather prediction model PBL schemes need to effectively simulate for accurate forecasting. Full recovery is defined as the time required for the postrainfall boundary layer to recover to its prerainfall boundary layer temperature and mixing ratio. We emphasize that the synoptic situations and rainfall amounts considered here are typical of the Great Plains during the summer months. We do not consider extreme situations such as prolonged low or high pressure systems that can lead to flood or drought conditions, and in which the speed of boundary layer recovery might be considerably different than in the three cases we have examined.

As part of this study, we examine the feedback of boundary layer clouds on surface processes with respect to the boundary layer circulations. We have based the study partly on measurements from a network of surface meteorology and energy budget stations, but mainly on a high vertical resolution radiosonde dataset obtained from the northwestern quadrant of the FIFE study area. The upper-air data, which were not used in the SEA94 study, provide some very compelling results concerning why the circulation was able to maintain itself throughout the course of IFC 5. In conducting this study, we provide a more complete explanation of how the secondary circulation originally detected in the SEA94 study, was modulated by larger-scale synoptic conditions.

In the remainder of the paper, we first describe the datasets used in the analysis (section 2) followed by a discussion of the sequence of synoptic events that occurred during IFC 5 (section 3). An analysis of the behavior of the secondary circulation is discussed in section 4, whereas the interrelationships of the circulation with land–atmosphere interactions are described in section 5. Conclusions are offered in section 6.

2. Description of datasets

For the purposes of this investigation, we have used four types of data that were archived and reside in the FIFE information system: 1) surface fluxes measured at

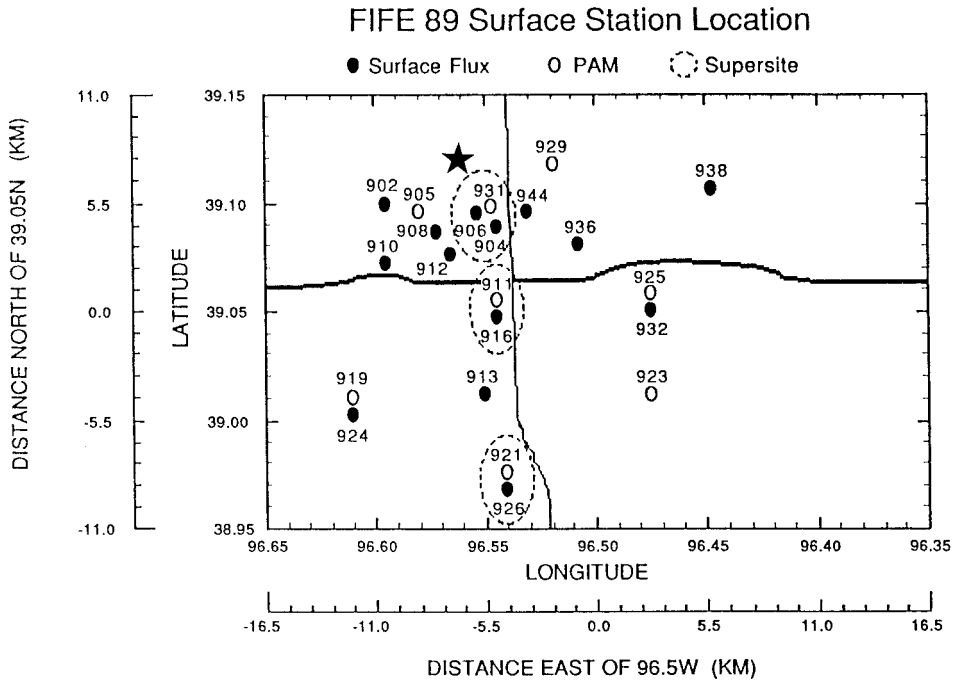

FIG. 1. Schematic layout of the 14 SFG and eight PAM stations along with the radiosonde launch site (indicated by the star) for IFC 5 period in 1989. The FIFE study area is divided into four quadrants by Interstate 70 (east–west highway indicated by thick black line) and State Road 177 (north–south highway indicated by thin black line).

surface flux group (SFG) stations; 2) meteorological variables measured at Portable Automated Mesonet (PAM) stations; 3) in situ soil moisture measurements; and 4) upper-air radiosonde measurements. Sellers et al. (1988, 1992) have described the basic instrumentation design, deployment strategy, measurement plan, and data acquisition procedures used for the IFCs. Here, we highlight features of the IFC 5 datasets used for this study. The 1989 IFC took place over the period from 23 July to 12 August.

The surface flux measurements were obtained from 14 SFG stations deployed over the 16 km by 16 km FIFE study area in 1989; see Fig. 1 and the article of Kanemasu et al. (1992) for further details on the 1989 SFG station configuration. Eleven of the 14 stations were instrumented with Bowen ratio systems, and three (stations 906, 916, and 926) used eddy-correlation sensors. In addition to the quantities of net surface radiation, soil heat flux, sensible heat flux, and latent heat flux, other quantities such as rainfall, temperature, and winds were recorded every 30 min at the SFG stations. The Kanemasu et al. article provides a full account of the instrumentation, computational methodologies, and calibration procedures used at the SFG sites. In this study, we make use of all surface flux and rainfall measurements obtained at these stations.

Operating eight PAM stations at the same half-hour sampling schedule, the National Center for Atmospheric Research (NCAR) obtained temperature, humidity, winds, rainfall, skin temperature, soil temperature at 10- and 50-cm depths, reflected solar radiation, and net radiation flux. Five of the PAM stations were collocated with SFG stations (see Fig. 1). More details can be found in the SEA94 article. In this study, we use the 10- and 50-cm soil temperatures, as well as the rainfall measurements.

During IFC 5, the in situ soil moisture measuring program included site specific measurements based on gravimetric sampling and neutron probe devices, along with aerial mapping based on remote sensing techniques (passive microwave L-band radiometry and natural gamma-ray emission). For this study, we use soil moisture obtained from the gravimetric samples in the 0–5-cm and 5–10-cm soil layers. These quantities, which are given as percentage soil moisture by mass, were taken regularly once per day at the SFG stations. The remotely sensed measurements were only obtained intermittently. The neutron probes were used to obtain deep soil moisture measurements down to 30 cm once per week at selected sites. However, because the deep measurements were not taken simultaneously, they are not easily assimilated into the upper-layer soil moisture analysis. For this reason, we have confined ourselves to the gravimetric measurements. Sellers et al. (1992) have provided a description of the observational procedures for obtaining soil moisture, while SEA94 discussed the reliability of the gravimetric measurements through com-

parison to the simultaneously acquired L-band and gamma-ray measurements.

The FIFE radiosonde launch site was located at 39.12°N and 96.56°W (Fig. 1) near the northern edge of the Konza Prairie Natural Area and west of Route 177, within the northwest quadrant of the study area. During IFC 5, the times of launch were between 0900 and 1800 CDT (0730 and 1630 solar time) at a rate of six–eight soundings per day. On rainy days, the number of launches was reduced to one–three soundings. The sounding reports usually terminated at about 5 km. In total, there were 80 soundings, only 73 of which could be used for this study. Seven soundings were rejected because of missing data problems and/or incomplete ascents. From the usable set of 73 profiles, soundings occur on 16 of the 21 IFC 5 days. No soundings were flown on 28 July and 9 August. Only one unusable sounding was flown on each of the three days 23, 27, and 29 July. Except for several of the lowest sounding levels, vertical resolution is typically 5 mb (~40–50 m). Each sounding includes pressure, geopotential height, u–v components of wind, dry- and wet-bulb temperatures, plus the derived quantities of potential temperature and mixing ratio. Descriptions of the sounding system used for collecting the upper-air measurements are found in Brutsaert and Sugita (1990), Brutsaert et al. (1990), and Sugita and Brutsaert (1990).

To composite the surface and upper-air measurements, knowledge of boundary layer height is required. Under cloudy skies, the common practice is to infer cloud base when dewpoint depressions are smaller than 5°C (e.g., Djuric 1994), whereas cloud top is estimated by identifying the level where there is a rapid increase in dewpoint depression, that is, the point where the sonde leaves the cloud layer. When we compared the results of this method to the 21-day IFC 5 sounding sequence with Brutsaert's field notes on cloud cover, types of clouds, and levels where the sondes first entered the clouds, we concluded that the 5°C cloud-base test was not stringent enough. We found that a smaller threshold of 2°C gave better correspondence to the field notes. Further details on determination of the cloud-topped boundary layer is given in the appendix.

As seen in Fig. 1, the radiosonde site was not collocated with any one of the SFG or PAM stations. Therefore, we selected six stations closest to the radiosonde site to represent surface conditions during radiosonde ascents. These are sites 902, 904, 906, and 908 from the SFG network, and sites 905 and 931 from the PAM network. Although large spatial gradients in the surface thermal and energy fields are found across the larger-scale FIFE study area (~30 km), the spatial gradients are small within the 2–3-km area containing the designated surface stations and the radiosonde site. The surface fluxes, soil moistures, soil temperatures, and rainfall accumulations from these six stations during the time frames of the radiosonde launches were arithmetically averaged to best represent surface conditions. As

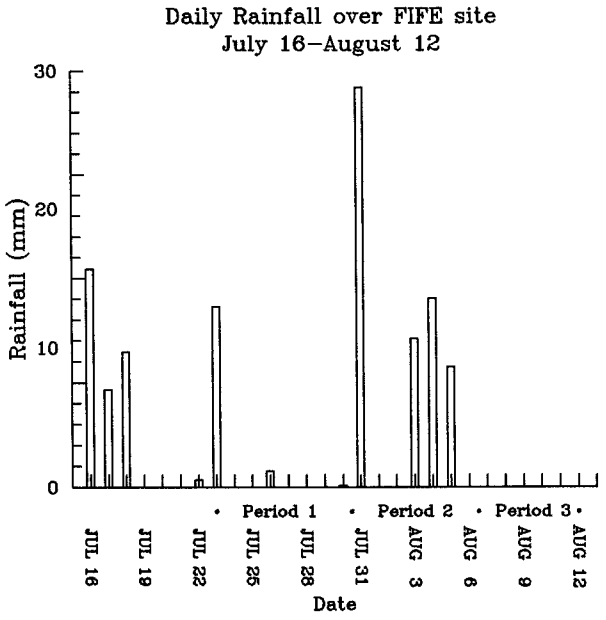

FIG. 2. Daily rainfall accumulation (mm) in the NW quadrant from 16 July to 12 August 1989, based on the four closest surface stations to the radiosonde site. The intervals of the three distinct synoptic events occurring during IFC 5 are indicated below the histogram.

the launch schedule times did not match exactly with the sampling times of the surface measurements, for purposes of discussion, we have set the time reference for each composite at the top of an hour. In the nomenclature used here, local times are indicted by an "h."

Our domain of study is some 2–3 km in the horizontal and about 2 km in the vertical. Therefore the measurements from the radiosonde below the boundary layer top, along with those of the selected surface stations, are representative of boundary layer conditions in the vicinity of the launch site. In essence, we are focusing on the ascending branch of the secondary circulation cell located over the FIFE study area.

3. Transition of synoptic events during IFC 5

Before discussing the behavior of the secondary circulation that generally persisted throughout the IFC 5 period, a description of the passage of synoptic events that took place during the course of IFC 5 is first given. This is helpful in proceeding with the discussions in sections 4 and 5. Figure 2 illustrates the daily sequence of accumulated rainfall for the week prior to and throughout IFC 5. This diagram should be referred to throughout the remainder of this analysis. As discussed in SEA94, rainfall was prevalent in the vicinity of the study area prior to the IFC, and had established a southeast–northwest aligned soil moisture–vegetation cover gradient that served to bring about a sustained secondary circulation across the FIFE site. The 23 July precipitation event on the first day of the IFC was associated

with a weather system passing through Kansas on 18 July. The cold 500-mb low pressure center of that system, which was over central Illinois on 21 July, began to retrogress westward on that day. By 23 July, it was over eastern Kansas giving rise to convective instability because of warm and moist flow beneath the upper-level low. The convection gradually decreased on 24 July as a strong 500-mb pressure ridge developed over the eastern United Sates, persisting through 28 July. The 500-mb pressure ridge finally weakened and moved off the United States east coast. Cumulus clouds were prevalent in the afternoons during this period. Midlevel and high-level clouds were also present throughout the day.

On 30 July, a surface pressure trough extended from New Mexico into northwest Kansas, stretching across the central plains into northwest Minnesota. The trough persisted through 31 July, producing extensive showers and thunderstorms associated with low-level convergence over the greater part of Kansas and Nebraska. Deep convective cloud systems including cumulonimbus, were a dominant feature on 30–31 July. On 1 August, the surface trough had dissipated and fair weather with cumulus clouds prevailed through 2 August. A surface low pressure center was located over southeast Alberta on 2 August. Associated with the low was a surface front that stretched across southwest Saskatchewan, eastern Montana, central Wyoming, northwest Utah, terminating in southern Nevada. Ahead of the front, a surface pressure trough brought showers to Kansas on 3 August. However, sunny and clear skies returned on 4 August. The surface cold front approached Kansas during the evening of 4 August, advecting through Kansas by 5 August. By 6 August, the site was under the influence of northerly flow behind the cold front. Clear skies persisted from 6 August through the morning of 7 August. The northerly flow began to shift when surface high pressure moved to the eastern seaboard. Toward the evening of 7 August, the surface flow in the central plains backed from northerly to westerly and then to southerly on 9 August. The general southerly flow remained for the rest of IFC 5. Boundary layer clouds were typically cumuliform. Mid- and high-level clouds were also present.

Although rainfall and showers were frequent during IFC 5 as seen in Fig. 2, Fig. 3 shows that about 40% of the soil moisture in the top 5-cm layer was removed by the third day after a rain event. Note the soil moisture in the top 10-cm layer becomes vertically uniform exactly three days after rain events that occurred on 18 July, 23 July, and 4 August (Fig. 3b). Also note that if there had been no rainfall on 3 August, exactly 3 days after the rain event on 31 July, the soil moisture in the upper 10-cm layer would have become vertically uniform. Beyond the third day after a rain event, soil moisture in the upper 5 cm dropped below the soil moisture in the deeper layer. These rapid changes in the upper-layer soil moistures indicate intense evapotranspiration rates.

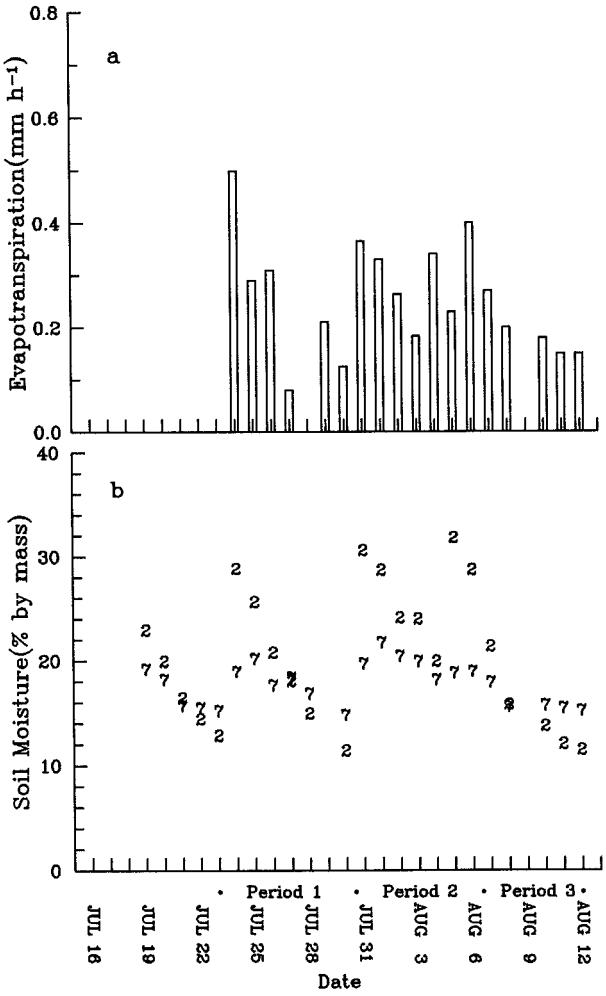

FIG. 3. Daily change in evapotranspiration (top panel) and soil moisture (bottom panel): (a) mean evapotranspiration (mm h^{-1}) corresponding to the radiosonde launch schedule, (b) daily soil moisture given in percentage by mass at 2.5 cm (symbol 2) and 7.5 cm (symbol 7). The intervals of the three distinct synoptic events occurring during IFC 5 are indicated below the bottom panel.

4. Behavior of FIFE IFC 5 secondary circulation

Initial inspection of the 73 quality-controlled IFC 5 soundings indicated the presence of microscale features. These represent high-frequency noise in conjunction with the scale of circulations being investigated. A vertical five-point filter was applied to the u- and v-components to remove these features. From the filtered profiles, the mean boundary layer wind profiles, $[u]$ and $[v]$, were then calculated for each day:

$$[u] = \frac{1}{N}\frac{1}{L}\sum_{z=1}^{N}\sum_{l=1}^{L} u(z, l) \quad (1)$$

for all 21 days

$$[v] = \frac{1}{N}\frac{1}{L}\sum_{z=1}^{N}\sum_{l=1}^{L} v(z, l), \quad (2)$$

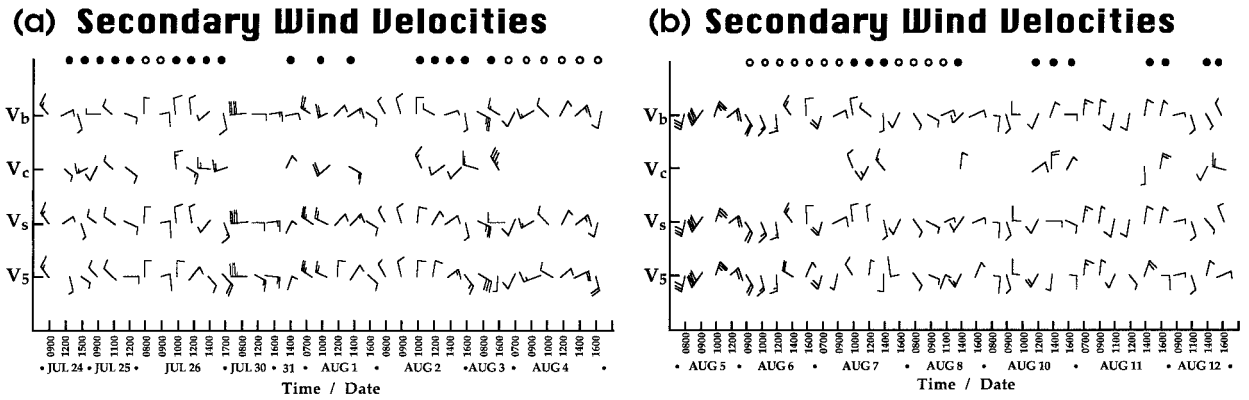

FIG. 4. (a) Averaged secondary wind velocity from 71 soundings during IFC 5 (24 July–4 August). Each full barb indicates a wind speed of 2 m s^{-1}. On top of each panel are symbols indicating sky conditions. Open circles indicate cloud cover is less than 0.1 including clear skies. Closed circles indicate a cloud-topped boundary layer. For days in which a symbol is not indicated, cloud conditions are variable. (b) Same as Fig. 4a except for period from 5 to 12 August.

where N is the number of vertical levels associated with each sounding and L is the number of launches, for a given day. Then, the perturbation u' and v' profiles for each sounding are given by

$$u'(z, l) = u(z, l) - [u] \quad (3)$$

$$v'(z, l) = v(z, l) - [v]. \quad (4)$$

For cloudy days, the daily mean boundary layer wind has been calculated twice based on two different values of N, the first for the number levels up to cloud base, the second up to cloud top. A comparative study of the two perturbation wind profiles associated with these two mean quantities will provide some insight on whether boundary layer cloudiness modifies the secondary circulation (see discussion below).

The u' and v' profiles are quite complicated. An examination of the profiles indicates that on perhaps 6 days, a wind direction reversal in the lower boundary layer can be found, indicative of the presence of a local secondary circulation. On most other days, such an interpretation is not obvious because of the complexities. On all but 2–3 days, the return branch of the circulation in the upper boundary layer cannot be found by examining the signs of u' and v', because the upper branch of such a perturbation circulation is so weak. Atkinson (1981) reported similar difficulties by a number of investigators in the detection of the return branch of the sea–land breeze circulation.

Because of the difficulties associated with interpreting the detailed perturbation profiles, we use four averaged quantities to examine the perturbation boundary layer winds. First the u'–v' quantities are averaged in the layer up to 500 m as a means to best represent perturbation conditions directly at the launch site. The time lapse to ascend to an altitude of 500 m was typically 2–3 min, so that with a mean boundary layer wind of ~5 m s^{-1}, a radiosonde would be carried downwind from the launch site about 1 km by the time it reached the 500-m level. Therefore, we can assume that the winds within 1 km of the launch site are generally representative of the boundary layer at the launch site. The vector wind associated with these averages of u' and v' is called $\mathbf{V}_5$. For the cloudy boundary layers, we obtain the average perturbation winds in the subcloud layer yielding $\mathbf{V}_s$. Also for cloudy boundary layer situations, we calculate the average perturbation winds for the cloud layer itself (from cloud base to cloud top), referring to this quantity as $\mathbf{V}_c$. Finally, we average the u' and v' components for the entire boundary layer, yielding $\mathbf{V}_b$. For boundary layers with either no cloudiness or variable cloudiness, the depth of the $\mathbf{V}_s$ and $\mathbf{V}_b$ layers are taken as equivalent, whereas $\mathbf{V}_c$ is simply not defined.

A comparison of the two sets of $\mathbf{V}_b$ and $\mathbf{V}_s$ quantities based on using the two different representations of the mean boundary layer winds (as described above for the two different N) did not reveal any significant differences. Therefore, for cloudy boundary layers, we have analyzed perturbation winds based strictly on the daily mean winds taken up to the top of the boundary layer (i.e., cloud-top height). Figure 4 depicts the secondary circulation structure by using wind barbs for the daily time series of $\mathbf{V}_5$, $\mathbf{V}_s$, $\mathbf{V}_c$, and $\mathbf{V}_b$, with $\mathbf{V}_s$ and $\mathbf{V}_b$ equivalent for cloud-free or variable cloud days. Sky conditions for each day are indicated above that day's set of wind barbs. Open circles indicate that cloud cover was less than 0.1 or that skies were completely clear. Closed circles indicate that the radiosondes were penetrating clouds within the boundary layer. The days for which no symbol is plotted represent situations in which the radiosondes did not penetrate boundary layer clouds, but there were partly cloudy skies over the FIFE domain. (Except for clear-sky cases, sky conditions include the influence of mid- and high-level clouds on the reports.) Considerable vertical shear in the boundary layer is indicated by progressive turning of the $\mathbf{V}_5$, $\mathbf{V}_s$, and $\mathbf{V}_b$ vectors.

Inspection of the time series of the perturbation layer-averaged wind speeds in Fig. 4 indicates the presence of a secondary circulation throughout the IFC, as reported by SEA94. The diurnal wind shift associated with the circulation occurred around midday or early afternoon. The periodicity of the wind shift was regular during 24–26 July, just before the period identified in the SEA94 analysis as being the least synoptically forced during IFC 5. Although the upper-air soundings were incomplete on 27 and 29 July, and no soundings were available on 28 July, it is presumed that the secondary circulation persisted through 29 July, because the synoptic-scale forcing did not change during this time, and it is recalled that the surface wind analysis and surface divergence pattern discussed in SEA94, indicated a strong secondary circulation during the period from 26–28 July. The secondary circulation on 30 July and 31 July was either masked or broken up by the passage of the surface trough in the vicinity of the FIFE domain over those two days. The wind shift from westerly to easterly on 30 July was related to that trough. A similar diurnal wind shift from the NW quadrant to the SE quadrant also occurred on 1 August. The secondary circulation was weak but present on that day, and then strengthened on 2 August, even though the diurnal wind shift did not take place until 1600 hours on those 2 days, some 2–3 h after its appearance on the synoptically quiescent days. The shower associated with the surface trough on 3 August again suppressed the secondary circulation temporarily. Clear skies returned on 4 August, as did the secondary circulation, even though there was an approximately 2-h delay in the diurnal wind shift, similar to 1–2 August.

The passage of the surface cold front was accompanied by a strong wind shift from southwesterly to northeasterly on 5 August. There is no evidence suggesting the presence of the secondary circulation on 5 and 6 August, likely because the rainfall and strong cold temperature advection disrupted the surface temperature gradient giving rise to the circulation. The secondary circulation returned on 7 August, albeit weakened, because northerly flow began to shift to westerly, and finally back to southerly on 9 August. The secondary circulation remained weak on 8 August (a case could be made from Fig. 4 that it was not actually present); no soundings were available from 9 August to establish the presence of a perturbation circulation, although it was likely similar to that of the previous day. During the last three days of the IFC (10–12 August), the secondary circulation had reestablished itself, although its behavior was sporadic and the periodicity of the diurnal wind shift was irregular. This was because the boundary layer was still in the process of recovering from the synoptically induced wind shift and the extended period of cold-air advection. By the end of the IFC, the boundary layer had yet to recover to its initial state, as potential temperature and mixing ratio deficits were 8°C and 7 g kg^{-1}, respectively.

TABLE 1. Summary of secondary circulation behavior during 21-day period of 1989 FIFE intensive field campaign.

IFC day	Date	Nature of secondary circulation
1	23 July	Probably present but no sounding data to verify
2	24	Pronounced
3	25	Pronounced
4	26	Pronounced
5	27	Pronounced (see SEA94)
6	28	Pronounced (see SEA94)
7	29	Probably present but no sounding data to verify
8	30	Disrupted
9	31	Disrupted
10	1 August	Weak with delayed wind shift
11	2	Pronounced with delayed wind shift
12	3	Disrupted
13	4	Pronounced with delayed wind shift
14	5	Destroyed
15	6	Destroyed
16	7	Weak and irregular
17	8	Weak and irregular or possibly disrupted
18	9	Probably present but no sounding data to verify
19	10	Pronounced but irregular
20	11	Pronounced but irregular
21	12	Pronounced but irregular

The above analysis shows that the diurnal reversal of the perturbation winds in the boundary layer near the northern edge of the FIFE domain exhibits a thermally direct secondary circulation consistent with the results described in SEA94. The return flow in the upper branch of the circulation is difficult to detect, although we can assume it exists given the clear evidence of the lower branch. The detection of the entire circuit is made difficult by the fact that a radiosonde network was not used for FIFE over a domain concomitant with the scale of the entire circulation cell. The circulation exhibits transient behavior due to synoptic disturbances, but it returns once a disturbance has passed over the FIFE site. The quantities $\mathbf{V}_5$, $\mathbf{V}_s$, $\mathbf{V}_c$, and $\mathbf{V}_b$ show a similar diurnal wind shift pattern during the day when the secondary circulation is present, indicating that boundary layer cumulus does not disrupt the perturbation flow. The passages of the surface trough and cold front either masked or broke up the circulation, but after both events, the preexisting secondary circulation returned after 1–2 days. In the case of the cold front, after the secondary circulation returned, it was irregular, likely because the boundary layer had not recovered to its prefrontal thermodynamic conditions. The intensive field campaign ended before boundary layer recovery was complete, so it was not possible to determine the behavior of the circulation after full recovery, although the intensity of the circulation was strong on the last day of the IFC. Table 1 summarizes the behavior of the secondary circulation on each of the 21 days of the entire 1989 IFC.

5. Interactions between secondary circulation and land surface processes

Seven sets of mean boundary layer quantities and four sets of soil-layer elements, along with the spatial av-

erages of surface fluxes are expressed in time series to depict the land surface–atmosphere interactions that took place in the boundary layer during the course of IFC 5. These quantities are boundary layer height (Z_i); potential temperature and mixing ratio at the surface (Θ_s, q_s), in the mixed layer (Θ_m, q_m), and in the cloud layer (Θ_c, q_c); soil temperatures in 10- and 50-cm layers (T_1, T_2); soil moistures at 2.5- and 7.5-cm depth (SM_2, SM_7); and surface fluxes of soil heat (G), sensible heat (H), latent heat (λ_E), and net radiation (R_n). The depth of the surface layer is taken as 10% of the boundary layer height. Diagrams of these time series are given in Figs. 5.1–5.4. To aid the following discussion containing numerical details on PBL conditions, Table 2 summarizes the behavior of the relevant variables at key times of the day.

a. Case of shallow boundary layer convection

After the rain event on 23 July, synoptic conditions were steady from 24 to 28 July. Because only one incomplete sounding was available on 27 July and no soundings on 28 July, the boundary layer conditions from 24 to 26 July have been selected to represent the undisturbed case. As indicated in Table 1, the secondary circulation during this period was well pronounced. Showers were frequent prior to and at the beginning of IFC 5, as shown in Fig. 2. Soil moisture levels had reached 20%–30% (by mass) in the upper 10-cm layer (Fig. 3b). The daily soil moisture gradually decreased, becoming vertically uniform on 27 July, beyond which SM_2 dropped below SM_7 until the end of the first period. Here, T_2 remained at 294.7 K throughout these three days.

The boundary layer on 24–26 July was under the influence of steady synoptic forcing. On 24 July, the top of a shallow, unstable boundary layer was located at 280 m at 0900 h (Fig. 5.1a). The value of T_1 was 294.8 K, differing little from T_2, indicating solar radiation had not yet heated the top soil layer (Fig. 5.1d). As time progressed, the boundary layer grew upward rapidly to 1400 m, with a cloud deck of 400 m at 1200 h, and finally to 1550 m with a cloud layer of 50 m at 1500 h. As indicated in Table 2, during a 6-h period, the boundary layer and upper soil-layer temperatures increased rapidly (Figs. 5.1c–d); Θ_s from 298.0 to 304.2 K, Θ_m from 296.9 to 302.9 K, and T_1 from 294.8 to 299.7 K. T_2 was steady with time. During the same time, the boundary layer mixing ratio decreased; q_s dropped from 14.1 to 12.2 g kg^{-1}, and q_m from 13.5 to 11.2 g kg^{-1} (Fig. 5.1b). Finally, Θ_c increased from 301.6 K at 1200 h to 303.5 K at 1500 h, while q_c decreased from 11.9 to 9.4 g kg^{-1}. Thus, the entire boundary layer warmed and dried with surface winds southerly throughout the day, and boundary layer winds southeasterly with little vertical shear.

On 25 July, the boundary layer and upper soil layers at 0900 h were slightly warmer and wetter than on the previous day (see top panel of Table 2): Θ_s = 298.9 K, Θ_m = 298.3 K, q_s = 14.9 g kg^{-1}, q_m = 14.5 g kg^{-1}, T_1 = 296.8 K, Θ_c = 299.3 K, and q_c = 13.8 g kg^{-1}. The boundary layer top was near 900 m at 0900 h, capped by a 600-m-thick cloud layer. At 1100 h, the cloud top lifted to 1075 m and cloud base lowered to 275 m. The surface and boundary layer winds were southwesterly under cloudy skies, somewhat similar to the previous day. The growth of the deepening cloud layer produced a negative feedback on the boundary layer. As indicated in Table 2 at 1100 h, T_1 had increased less than 1°C. The boundary layer changed over from unstable to stable as Θ_s decreased to 297.8 K while Θ_m and Θ_c remained almost constant (298.3 and 299.5 K, respectively). Since increased surface stability prevented turbulent transport from accumulating surface moisture into the subcloud layer, q_s and q_m increased to 15.8 and 14.8 g kg^{-1}, respectively. As the cloud layer grew thicker, R_n, H, λ_E, and G dropped at the surface (Figs. 5.1e–h). If the subcloud layer had maintained buoyancy and continued to moisten, the buoyant and moistening effects below cloud base might have been able to sustain the cloud layer and its growth, in spite of the reduction of the surface heat and moisture fluxes. However, when the deficits of heat and moisture due to increased stratification in the subcloud layer were not compensated by some other means such as advection, the cloud layer eventually dissipated.

Between 1100 and 1200 h, the deep cloud layer broke up, changing from heavy dark towering cumulus with cloud cover of 0.7–0.8, to cumulus humilus with cloud cover of 0.5 and strong sunshine (according to Professor Brutsaert's cloud log). This resulted from the loss of buoyancy due to stabilizing effects, as indicated by subcloud temperatures. Accompanying the breakup of the cloud layer were rapid changes in surface and boundary layer quantities (see Table 2). Jumps occurred in air and soil temperatures with drops in mixing ratios: Θ_s = 303.2 K, Θ_m = 302.2 K, Θ_c = 302.9 K, q_s = 14.2 g kg^{-1}, q_m = 13.1 g kg^{-1}, q_c = 11.6 g kg^{-1}, and T_1 = 298.7 K. Surface fluxes increased rapidly and the boundary layer top grew nearly another 200 m to 1370 m. Surface winds maintained southwesterly flow while boundary layer winds shifted to southeasterly.

Boundary layer conditions on 26 July were similar to those of 24 July (warm, moist, and unstable). At 1200 h, Z_i grew to 2220 m, capped with a 100-m thick cloud layer, about 870 m deeper than at the same time on July 24 (1350 m). Clouds persisted in the unstable boundary layer during the day. By 1700 h, Z_i settled to 1900 m, retaining a 100-m thick cloud layer. The entire boundary layer was 2°–3° warmer and 1–2 g kg^{-1} moister than on 24 July, even though surface heat fluxes on both days were similar.

To gain insight into what mechanism produced the additional boundary layer heating, we estimate the relative importance of turbulence heating and warm temperature advection from mixed layer theory. Around

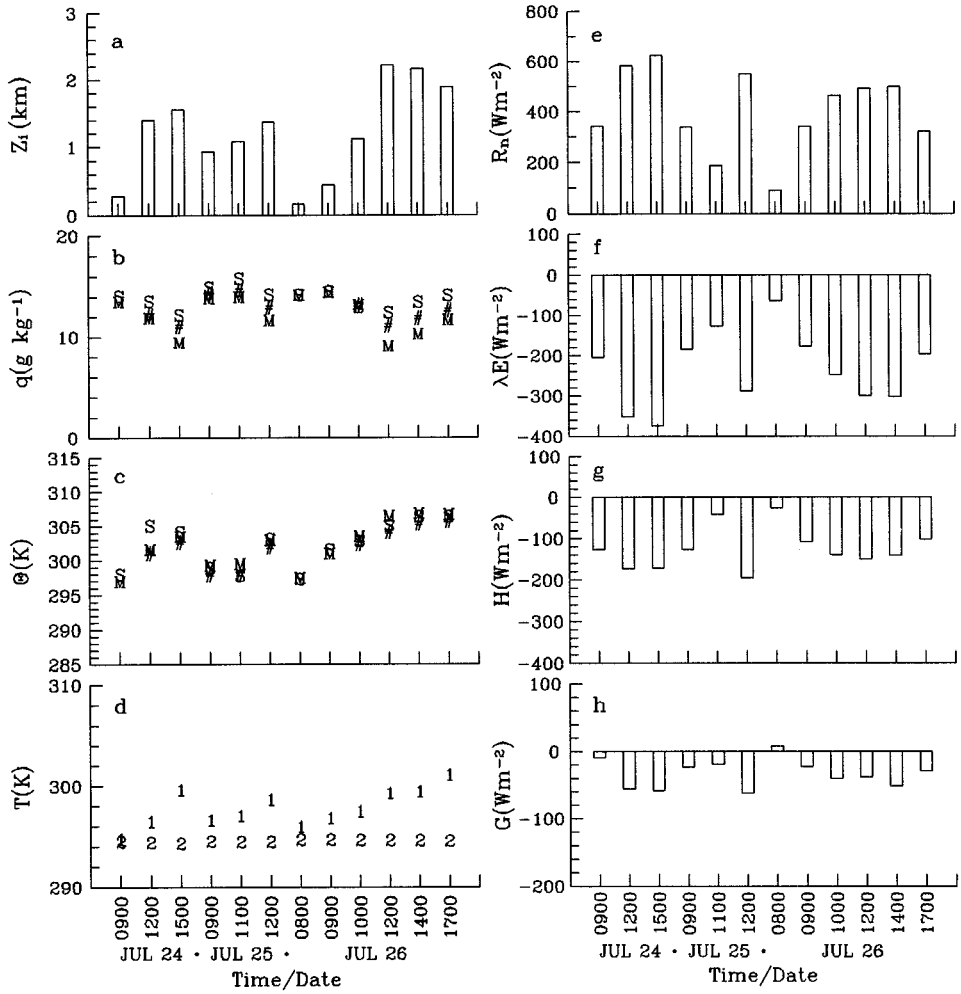

FIG. 5.1. Daily structures of soil profile and boundary layer for the period 24–26 July: (a) boundary layer height (Z_i) in km, (b) mixing ratio (q) in g kg^{-1}, (c) potential temperature (Θ) in K, (d) soil temperature (T) at 10 cm (symbol 1) and 50 cm (symbol 2) in K, (e) net surface radiation (R_n) in W m^{-2}, (f) latent heat flux (λ_E) in W m^{-2}, (g) sensible heat flux (H) in W m^{-2}, and (h) soil heat flux (G) in W m^{-2}. For the q and Θ panels, the symbols M, S, and # indicate mixed layer, surface layer, and cloud layer, respectively.

1000 LT skies are clear, with the boundary layer exhibiting uniform conditions and small radiative flux divergence. Therefore, any residual in the temperature budget equation can be attributed to advection. A temperature change resulting from turbulent heating is given by $(\overline{w\theta})_o/(\rho C_p Z_i)\Delta t$, where $(\overline{w\theta})_o$ is surface heat flux in W m^{-2}, Δt is the time period under consideration in seconds, ρ is air density (1.275 kg m^{-3}), and C_p is 1004 J K^{-1} kg^{-1}. At 0900 h, $(\overline{w\theta})_o$ = 108 W m^{-2} and Z_i = 443 m. The temperature change due to turbulent heating up until 1000 h would have been 0.8°C. The observed temperature change over that 1-h time interval was 1.7°C. Therefore, the additional heating must have resulted from warm temperature advection, possibly from a source in the Gulf of Mexico, ultimately producing the deeper boundary layer.

Besides cloud cover, available soil moisture had an important effect on the surface energy balance and boundary layer energetics. From 24 to 26 July, midday R_n was relatively constant between 550 and 600 W m^{-2}. The partition of R_n into sensible heating for boundary layer growth, evapotranspiration (ET), and storage in the soil layers was somewhat different on these three days, although most of R_n was balanced by latent heat flux. For instance considering the 3-day mean, at 1200 h near peak solar insolation, about 58% of R_n went into ET. For cloudy sky conditions at 1100 h on 25 July the ET use rate was up to 67%. From a discrete sample of latent heat fluxes at the times corresponding to the launch times of the radiosondes (when cloud reports were available), the day-by-day averaged evapotranspirative mass fluxes were 0.45, 0.29, and 0.31 mm h^{-1} for the three consecutive days (Fig. 3a), a variation of some 40% with respect to the average 3-day mass flux. About 33% of R_n (considering the 3-day mean) was used for sensible heating of the boundary layer and its

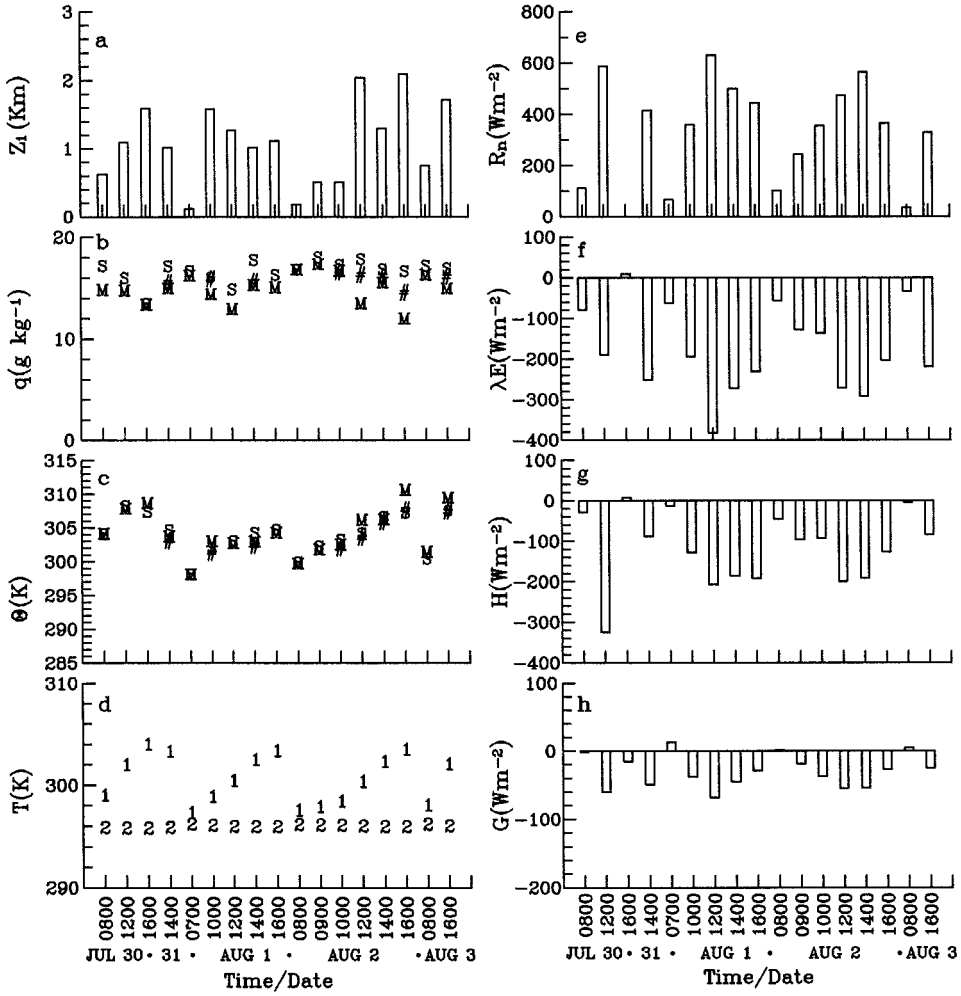

FIG. 5.2. Same as Fig. 5.1 except for the period 30 July–3 August.

growth, but without much day-to-day variability in the surface sensible heat flux. The somewhat wet surface and accompanying ET, regardless of its variability, kept the surface temperatures relatively cool and the boundary layer cool and moist. During the 3-day period, about 9%–10% of daytime R_n was stored in the upper soil layers, a fairly typical value for daytime G.

In summary, the shallow cumulus clouds for the undisturbed 24–26 July situation, during which the secondary circulation was relatively intense, appeared to have had no adverse effects on the maintenance of the circulation in spite of their strong influence on the surface energy balance and boundary layer energetics. Presumably this depended upon boundary layer dynamics and thermodynamics feeding moisture and buoyancy into the clouds. The secondary circulation is, in essence, a manifestation of boundary layer dynamics and thermodynamics. When a cloud layer has grown too deep, it may cut off its heat and moisture sources from the surface. If there are no other mechanisms, such as advection or moisture convergence, providing buoyancy and moisture to sustain the convection, clouds often dissipate allowing the preexisting secondary circulation to continue. By the same token, a secondary circulation can advance to the stage where it affects the maintenance of boundary layer clouds. This has been noted for the case of stratocumulus. For this situation, if the ascending branch of the secondary circulation enhances the growth of the boundary layer, entrainment of dry, warm air from above the cloud layer can break up the cloud deck into individual clouds; see Kuo and Schubert (1988), Siems et el. (1990), and Wai (1992).

b. Case of surface trough passage

On 30 July and again on 3 August, days on which the secondary circulation was disrupted, a surface trough was located west of the FIFE domain. The surface trough not only maintained warm and moist southerly flow, which persisted throughout 30 July to 4 August, but also led to large-scale low-level surface convergence, bringing extensive rainfall to the FIFE domain

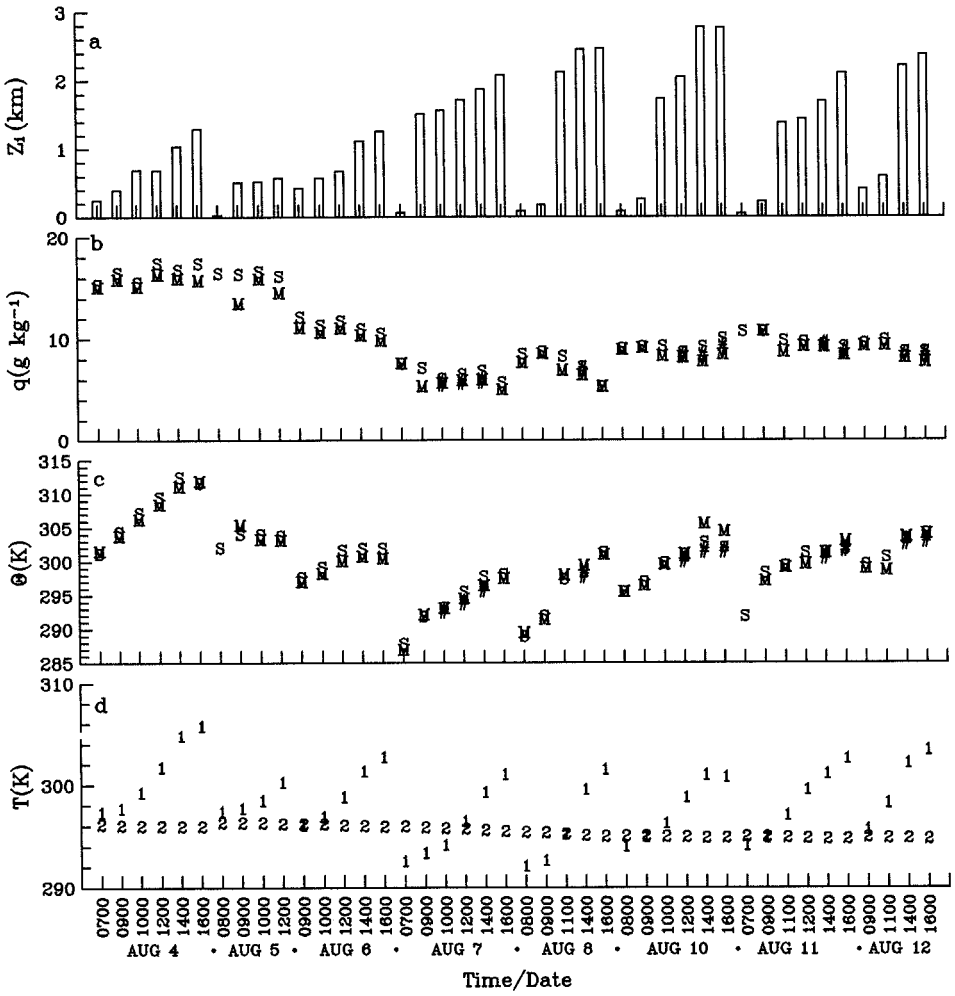

FIG. 5.3. Same as Fig. 5.1 except for the period 4–12 August and including only the Z_i, q, Θ, and T panels (no radiosondes were launched on 9 August).

on the morning of 31 July and light rain on 3 August. During this 6-day period, the mean boundary layer and soil layers were warmer and wetter than those of the undisturbed period. For instance, the mean value of T_2 of 297 K was almost 2°C warmer.

The boundary layer on 30 July was convective in nature. Soil moisture in the upper 50 cm fell below 12% (Fig. 3b). Between 0800 and 1200 h, Z_i rose from 500 m to 1 km (Fig. 5.2a). The boundary layer and soil layers had undergone warming and drying (Figs. 5.2b–d) with Θ_s changing from 304.2 to 308.3 K, Θ_m from 304.2 to 307.8 K, T_1 from 299.1 to 302.2 K, and although q_m did not change, q_s changed from 17.2 to 15.9 g kg^{-1}. The middle panel of Table 2 summarizes these changes. At 1200 h, where T_1 reached a value of 302.2 K (Fig. 5.2d), corresponding to a minimum value of SM_2, which actually fell below the value of SM_7 (Fig. 3b). At this time, a large fraction of R_n (55%) was supplying boundary layer heating, while only 32% of surface R_n was going into ET (0.13 mm h^{-1}). Consistent with SM_2 dropping below SM_7 and the accompanying drier surface, ET rates were reduced substantially compared to those during the undisturbed 24–26 July period.

Since increased boundary layer temperature and height on 30 July increased linearly with time, we can assume that vertical motion and entrainment were the two principal mechanisms responsible for its growth (Stull 1988) and estimate the relative importance of these two mechanisms. Based on a quadratic equation of the vertical motion, which is expressed in terms of perturbation surface divergence and height as given in SEA94, the estimated mean vertical velocity near the mean inversion base (1102 m) was about 0.98 cm s^{-1} at 1200 h. The mean vertical motion would increase Z_i by 302 m over an 8-h period. The observed mean increase in Z_i for the 0800 h to 1600 h interval was about 483 m, meaning that entrainment at the inversion base led to an increase of about 181 m in the growth of Z_i, or about 40% of the total. The other 60% of the growth in Z_i can be attributed to ongoing boundary layer cir-

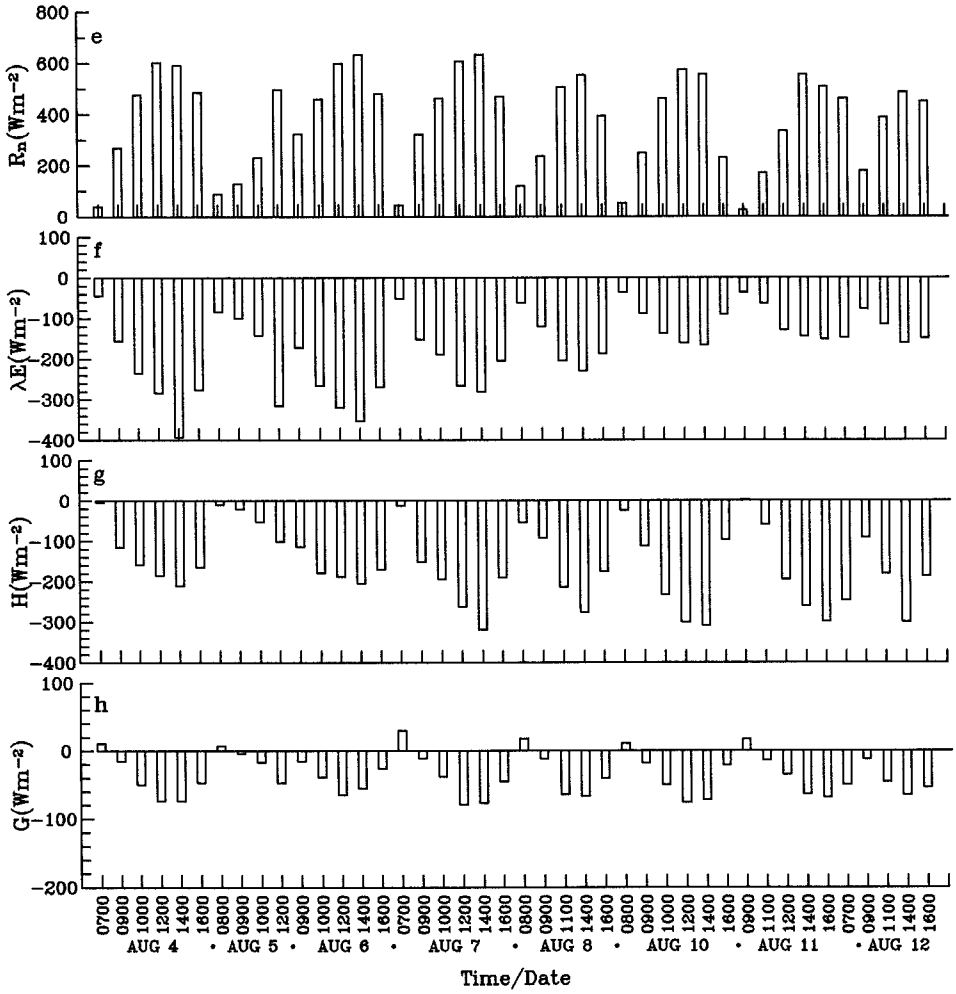

FIG. 5.4. Same as Fig. 5.1 except for the period 4–12 August and including only the R_n, λ_E, H, and G panels (no radiosondes were launched on 9 August).

culations, possibly even a disrupted manifestation of the secondary circulation, but too disorganized to recognize from the perturbation analysis.

On 30 July between 1500 and 1800 h, light, scattered showers occurred in the northern and western quadrants of the FIFE study area. This did not replenish soil moisture to any great degree. At 1600 h, the boundary layer stabilized with Θ_s = 307.4 K and Θ_m = 308.7 K, with the boundary layer top at 1500 m. The effect of the rain on the surface can be seen by the drop of surface layer temperature and the moisture quantities, as both q_s and q_m dropped to 13.5 g kg^{-1} (see Table 2). Notably, the fluxes of R_n, H, λ_E, and G all dropped, while H and λ_E changed signs (Fig. 5.2e–h).

Between 0200 and 1000 h on 31 July, the second day of the surface trough passage event when the secondary circulation was disrupted, large-scale low-level convergence over the greater part of Kansas and Nebraska produced extensive rainfall over the FIFE domain. SM_2 increased to about 30% and SM_7 increased to 20%. The upper soil layers remained relatively wet through 3 August. Note that the light rain on the morning of 3 August (Fig. 2) did not change the soil moisture contents significantly (Fig. 3b). The boundary layer top at 1400 hours was located at 1 km, which was relatively low as compared to that on 30 July. Also, compared to the previous day, the boundary layer and soil layers were cooler and wetter with T_1 = 303.4 K, Θ_s = 304.7 K, q_s = 17.2 g kg^{-1}, Θ_m = 303.4 K, Θ_c = 303.8 K, q_m = 15.7 g kg^{-1}, and q_c = 14.9 g kg^{-1}.

A sharp reversal in the roles of sensible and latent heat fluxes on boundary layer energetics was evident over the 24-h cycle between 1200 h on 30 July and 1200 h on 31 July. Prior to the extensive rainfall, about 57% of R_n was used for sensible heating while 32% was used for ET. After the July 31 rainfall event, 22% of R_n was used for sensible heating while 67% was used for ET at a rate of 0.37 mm h^{-1} (Fig. 3a). About 10% of R_n went into soil heat flux throughout the rain cycle. Since the ground was wet, the thermal heat capacity of the

TABLE 2. Summary of values of boundary layer variables during key times on 24–25 July (top panel), 30 July (middle panel), and 4 and 7 August (bottom panel). The asterisks for Θ_c and q_c on 24 July indicate no cloud was present at that time. Times are CDT.

	24 July			25 July		
	0900	1200	1500	0900	1100	1200
Z_i(m)	280	1400	1550	900	1075	1370
Θ_s(K)	298.0	305.2	304.2	298.9	297.8	303.2
q_s(g kg^{-1})	14.1	13.6	12.2	14.9	15.8	14.2
Θ_m(K)	296.9	301.3	302.9	298.3	298.3	302.2
q_m(g kg^{-1})	13.5	12.4	11.2	14.5	14.8	13.1
Θ_c(K)	*	301.6	303.5	299.3	299.5	302.9
q_c(g kg^{-1})	*	11.9	9.4	13.8	13.9	11.6
T_1(K)	294.8	296.2	299.7	296.8	297.3	298.7

	30 July		
	0800	1200	1600
Z_i(m)	500	1000	1500
Θ_s(K)	304.2	308.3	307.4
q_s(g kg^{-1})	17.2	15.9	13.5
Θ_m(K)	304.2	307.8	308.7
q_m(g kg^{-1})	14.8	14.8	13.5
T_1(K)	299.1	302.2	303.5

	4 August	7 August
	1200	1200
Z_i(m)	690	1720
Θ_s(K)	309.6	295.1
q_s(g kg^{-1})	17.4	6.5
Θ_m(K)	308.4	294.3
q_m(g kg^{-1})	16.3	5.9
T_1(K)	301.8	296.5

upper soil layers was large relative to dry-down days; therefore soil temperatures did not increase as rapidly as they did on the drier days. By the following day (1 August), the surface trough dissipated and fair weather, along with the secondary circulation, prevailed through 2 August. During the first two days of August, the surface and boundary layer winds were initially southeasterly, later shifting to more southerly.

The boundary layer returned to unstable conditions on 1 August. That day began with a shallow stable layer at 0700 h because the surface was still wet and relatively cool after the heavy precipitation on the previous day. By 1400 h, the boundary layer had grown to nearly 1 km. Although the boundary layer warmed, Θ_m and Θ_s were still about 5° cooler than on 30 July; these quantities changed very little the rest of the day. To determine the effect of the cool and wet surface on the boundary layer, we repeat the calculation of the boundary layer temperature change due to turbulent heating. Using $(\overline{w\theta})_o = 207$ W m^{-2} and $Z_i = 1271$ m at 1200 h, the boundary layer temperature would have increased 0.8° in 2 h. However, the observed Θ_m increased only 0.4°C. Therefore, we expect that turbulent warming was partially offset by the advection of cool air over a long fetch of cool and wet surface.

The warming trend continued to 1600 h on 2 August. Boundary layer temperatures eventually reached values of $\Theta_s = 307.2$ and $\Theta_m = 307.9$ K, very similar to those on 30 July. However, the values of q_s and q_m throughout 1–2 August were consistently larger than those of 30 July by 1–3 g kg^{-1}. Unlike 1 August, the effect of a cool and wet surface on the boundary layer was not as pronounced on 2 August. To verify this deduction, we calculate the change in boundary layer temperature at 0900 h due to turbulent warming. We use $(\overline{w\theta})_o = 96$ W m^{-2} and $Z_i = 510$ m. This results in a 0.72°C increase in boundary layer temperature in 2 h. The observed temperature change was 0.51°C. Therefore, turbulent heating accounted for almost all of the temperature change. It is noted that ET dropped from 0.36 m h^{-1} on 31 July to 0.26 mm h^{-1} on 2 August. The decrease and the accompanying increased sensible heating led to a more normal onset of the diurnal wind shift as compared to that which occurred on 1 August.

On 3 August, rainfall again broke up the secondary circulation temporarily. A similar situation to the previous event in which ET dominated over sensible heating was the root cause. By the following day (4 August), the ET rate dropped, sensible heating picked up, and the secondary circulation returned.

In summary, the boundary layer responded quickly to the major rainfall events of 31 July and 3 August, both associated with the passage of a surface trough. During the events, the surface layer collapsed and decoupled from the mixed layer. The boundary layer temperatures fell, and the sensible heat flux dropped and changed sign. Evapotranspiration also stopped momentarily as indicated by the change in sign of the latent heat flux. Because of this external forcing on the boundary layer, the secondary circulation ceased to exist. After the rainfall events, the boundary layer began its recovery with vigorous ET rates removing excess water in the upper soil layers on a timescale of 1–2 days. As the soil moistures dropped, sensible heating became more dominant in governing boundary layer energetics. This marked the return of the secondary circulation and the accompanying delay in the diurnal wind shift. For the boundary layer to recover to its initial undisturbed state, it needed at least 2 days, presuming that the surface trough did not bring about a reversal in the direction of the boundary layer winds (this issue will be discussed further in section 5c).

The preexisting secondary circulation probably can fully reappear only after a complete recovery of the boundary layer. Viewing the detailed behavior of boundary layer thermodynamics during the passage of the surface trough indicates that the boundary layer did not exactly recover to its initial state (i.e., the conditions of 30 July). This denotes how the atmosphere is constantly producing its own fluctuations through nonlinear adjustments of land surface–atmosphere interactions leading to ever changing boundary layer structures. Nevertheless, such interactions during the FIFE IFC 5 period were not able to fully break down and destroy the secondary circulation.

c. Case of surface cold front passage

Clear weather returned on 4 August. That day began with a stable boundary layer at 0700 h; after 0900 h, Z_i had grown to 1300 m (Fig. 5.3a). At 1200 h, as indicated in the bottom panel of Table 2, Z_i = 690 m, Θ_s = 309.6 K, Θ_m = 308.4 K, q_s = 17.4 g kg^{-1}, q_m = 16.3 g kg^{-1}, and T_1 = 301.8 K (Figs. 5.3a–d). The secondary circulation returned although with an extended delay in the diurnal wind shift (see section 4). The vertical extent of the circulation was about 500 m. Evapotranspiration on that day was consuming most of the net radiation flux.

Frontal rainfall began on the evening of 4 August and into the morning of 5 August. The rainfall decreased as the surface cold front passed through the FIFE domain (Fig. 2). There was a sharp wind shift from southwesterly to northeasterly. The boundary layer cooled but the surface remained wet. Surface fluxes decreased because of the combination of cloud cover, a wet surface, and cold temperature advection (Figs. 5.4e–h). The rainfall elevated SM_2 back to 30% (Fig. 3b), but SM_7 increased less than 1% indicating the soil layer below 5 cm was still saturated. After the frontal passage, SM_2 dropped steadily and eventually matched that of SM_7. On 8 August SM_2 fell below SM_7, remaining so until the end of IFC 5. On 5–6 August, ET rates were high (0.34–0.4 mm h^{-1}), removing excess water in the upper soil layers. The rates decreased to 0.15–0.18 mm h^{-1} by the end of IFC 5.

Sunny and clear skies prevailed on 6 August, with strong cold temperature advection the dominant feature. Above the boundary layer, an upper-level inversion located at 1600 m appeared, persisting the following 3 days. The associated nocturnal cooling produced a shallow surface stable layer throughout the mornings of 7–10 August. This layer eroded and merged with the upper-level boundary layer around midday. Therefore, it required a longer time for turbulent heating to warm boundary layer air.

Although solar radiation managed to heat the boundary layer, turbulent heating could not overcome the cooling due to cold temperature advection behind the cold front. To illustrate, we calculate the temperature change due to turbulent heating. On 6 August around 1200 h, turbulent heating would have increased boundary layer temperature by 1.5°C in a 2-h period. However, the actual temperature increase was only 0.5°C. Therefore, cold temperature advection offset most of the turbulent heating. The effects of cooling and drying on the boundary layer and soil lasted until late morning of 9 August. Although T_1 fluctuated diurnally, T_2 decreased gradually to the end of IFC 5 (Fig. 5.3d). Soil temperatures, boundary layer temperatures, and mixing ratios reached their minimum values on 7 August. For instance at 1200 h (see Table 2), Θ_s = 295.1 K, Θ_m = 294.3 K, q_s = 6.5 g kg^{-1}, q_m = 5.9 g kg^{-1}, and T_1 = 296.5 K. Boundary layer height was 1720 m. Here, T_1 was colder than T_2 for two consecutive days from 7 to 8 August, and did not climb above T_2 before 1200 h. The secondary circulation reappeared on 7 August around 1400 h, although weak and irregular.

The postfrontal warming trend began on 8 August as the synoptic system began moving to the east. At that point, cold temperature advection gradually receded. Accompanying the warming trend was a shift of the surface winds to westerly, and finally southerly flow on 9 August. At the end of IFC 5 (12 August), the boundary layer had still not recovered to its initial state of 4 August, as indicated by the ambient boundary layer temperature and mixing ratio quantities. Moreover, the secondary circulation, which had returned by 7 August and strengthened on 10 August, was sporadic in nature.

In summary, the external forcing on the boundary layer brought about by the passage of the surface cold front suppressed the secondary circulation for a few days. The immediate effect of strong cold temperature advection was to overwhelm boundary layer processes, probably to the extent of destroying the secondary circulation. The cooling of the land surface in response to the passage of the surface cold front also reduced the heating of the boundary layer. When cold temperature advection receded, combined with increased sensible heating, the secondary circulation reappeared. At first it was weak with a lengthened delay in the diurnal wind shift. Thereafter it strengthened but was sporadic, because even though the ambient background flow returned to southerlies, the boundary layer temperature and moisture levels were still adjusting to the effects of cold air advection. Before the boundary layer fully recovered and the secondary circulation could settle, IFC 5 ended and the analysis was terminated.

6. Conclusions

Further evidence of a persisting secondary circulation has been found from analysis of upper-air measurements obtained during FIFE IFC 5. Consistent with analysis of surface winds from the SEA94 study, the secondary circulation is found to be thermally direct in nature with vertical extent of at least 500 m. The circulation is sustained by a northwest–southeast aligned gradient in surface temperature, which resulted from biophysical feedback associated with variable vegetation cover and evapotranspiration. The persistence and breakup of the circulation depended on boundary layer dynamics and the prevailing larger-scale synoptic circulation.

The secondary circulation can survive the formation of shallow convective clouds provided that the cloud layer does not weaken the horizontal temperature gradient by stabilizing the surface layer beneath the clouds. When the clouds have grown too deep, a regulatory process transforms the boundary layer from unstable to stable and results in inhibiting the supply of heat and moisture from surface to atmosphere. For the shallow convection event examined here, the increased stratifi-

cation in the boundary layer suppressed the secondary circulation without destroying it, as the horizontal temperature gradient weakened. With no other mechanism to feed heat and moisture into the clouds, the breakup of the cloud layer occurred, thus allowing the secondary circulation to reintensify and continue.

Heavy rainfall and cold temperature advection are found to break up the secondary circulation. Surface rainfall produces a progression of impacts on the boundary layer: 1) collapse of the surface layer, 2) falls in the surface and soil layer temperatures, 3) reduction of surface fluxes, and 4) temporary suspension of evapotranspiration. After a rain event associated with the passage of a surface trough, the boundary layer began its recovery with intense evapotranspiration removing excess water from the upper 10 cm soil layer on a timescale of 1–2 days. This timescale is regulated by the preexisting soil water content, particularly deep soil moisture. As soil moisture decreased after passage of the trough, surface sensible heating became more effective in controlling boundary layer energetics. The secondary circulation returned after 2 days. Its initial return was marked by a delay of the wind shift during the midday, relative to the more synoptically quiescent days of IFC 5.

In the case of dissipation of shallow convective clouds, the boundary layer recovered on a timescale of several hours. In the case of the surface trough, the boundary layer temperature and moisture required approximately 2 days to recover to its initial state. In the case of the surface cold front because of the reversal of the direction of prevailing winds, the boundary layer did not fully recover for at least a week, although the secondary circulation returned within two days of frontal passage. It should be noted that the boundary layer seldom recovers exactly to its initial state after any type of synoptic disturbance because nonlinear land surface–atmospheric interactions are constantly producing their own self-adjusting fluctuations.

This study shows that biophysical induced forcing of the boundary layer associated with an organized vegetation cover gradient is capable of sustaining a mesoscale circulation feature within a domain of ~ 16 km^2 even after passage of convective cloud development or even after synoptic rainstorm events. Since higher vertical and horizontal resolution have partly contributed to the steady improvement in the skill of large-scale forecasts (Anthes 1983), it would make sense to include a variable fine mesh in state-of-the art large-scale models, such as described by Gravel and Staniforth (1992), in order to determine if prediction skill can be improved by resolving such mesoscale features as investigated here.

Acknowledgments. The authors wish to thank Professor Wilfried Brutsaert of Cornell University for kindly providing us with copies of his field notes and cloud logs for the radiosonde flights that he diligently launched during IFC 5. This research has been supported by NASA Grants NAG5-891, NAGW-1840, and NAG5-2072. A portion of the computational support has been provided by the Supercomputer Computations Research Institute at The Florida State University under DOE Contract DE-FC05-85ER250000.

APPENDIX

Identification of Cloud-Topped Boundary Layer

There are standard procedures that use surface observations of cloud cover along with boundary layer profiles of temperature and relative humidity to estimate the lower and upper levels of a cloud-topped boundary layer (see Djuric 1994). We found that the standard procedures were somewhat unsatisfactory in locating boundary layer clouds when applied to the northwest sector of the FIFE study area. First, cloud cover observations by themselves do not indicate the horizontal location of clouds in the celestial dome, except for a completely overcast sky. Furthermore, the packing effect appears to make clouds more numerous than they really are near the horizon. It is virtually impossible for surface observers to make allowance for an effect they cannot discern; therefore they report sky cover on the basis of the amount of sky ''apparently'' covered. Furthermore, although cloud-base heights are estimated from what is observed overhead, conventional surface observations do not contain any quantitative information on the vertical extent of clouds. Consequently, sky cover alone is not sufficient as an indicator of the vertical position of a cloud-topped boundary layer.

Theoretically, using simple principles of moist thermodynamics for horizontally homogeneous atmospheres, the locations of cloud layers can be deduced from radiosonde observations of temperature and humidity, assuming the sondes have penetrated the clouds. In practice, one finds that such determinations are not always reliable. There are several reasons for this. First, there are instances where condensation may occur below 100% relative humidity in the presence of larger hygroscopic aerosols, or because cloudiness is not generally horizontally homogeneous, the radiosondes may penetrate gaps within the clouds or along cloud edges. Accordingly, the relative humidities will be too far below saturation to indicate the presence of cloud layers. Second, temperature and humidity sensors on most radiosondes undergo time lags before adjusting to the changing ambient temperature and moisture conditions (see Luers and Eskridge 1995; Connell and Miller 1995). This is particularly true for humidity sensors whose time lags can exceed 15 s (WMO 1983). The time lags for the dry- and wet-bulb sensors on the sondes used for FIFE soundings were 3 and 12 s, respectively (Sugita and Brutsaert 1990).

For humidity sensors, the adjustments follow an exponential decay rule in which the constants of the exponential expression depend on the rate of change of

both temperature and humidity. It is difficult to correct for these time lags when using radiosonde measurements for determining thermodynamic structure, except in an empirical manner. Furthermore, the time lags increase with decreasing temperature. Therefore, time lags are largest when sondes pass from warm dry air into cold moist air, which is the characteristic transition from a subcloud layer into the cloud layer. Furthermore, humidity sensors are vulnerable to degradation and hysteresis during ascent when passing through cloud media. Some sensor elements, such as lithium chloride, become wetted and washed out within cloud environments, resulting in reported values of humidity that are too low (Bunker 1953). The majority of humidity sensors on operational radiosondes are carbon-coated plastic elements in which the transducer is based on the carbon element's resistive property changing to changing humidity (Connell and Miller 1995). At high humidities and in the presence of liquid water, the carbon granules become wetted and less binding, resulting in abnormally increased resistance, which leads to erroneously lower values of relative humidity inside the cloud (see Golden et al. 1986).

A common practice to infer cloud layer positions from radiosonde measurements is based on empirical tests associated with the dewpoint depression (T_d) (Djuric 1994). The following standard thresholds have been derived from aircraft observations taken in the vicinity of radiosonde ascents: 1) T_d's between 0° and 2°C indicate overcast skies; 2) T_d's between 2° and 5°C indicate scattered to broken clouds; and 3) T_d's greater than 5°C indicate widely scattered clouds or clear skies.

When we compared results from these empirical tests with the field notes collected by Professor Brutsaert during the FIFE radiosonde ascents, which include reports on cloud cover, types of clouds, and levels where the sondes entered and exited the clouds, we find that thresholds 2 and 3 are too large. Therefore, we modified the original rules to more stringent thresholds, verifying the rules by intercomparing the location of the boundary layer tops with the field notes of the radiosonde flights. The modified rules are as follows: 1) a well-developed cloud-topped boundary layer is indicated by T_d's in the 0°–2°C range once the sonde penetrates a cloud layer; 2) variable cloudiness in the boundary layer is indicated by T_d's in the 2°–3°C range; and 3) T_d's greater than 3°C or more indicate no boundary layer clouds are present. Therefore, for the FIFE analysis, cloud bases are located at levels where the dewpoint depressions are equal to or less than 2°C, whereas cloud tops are located at levels where the dewpoint depressions increase rapidly and exceed 2°C. Using the modified rules, we have inferred the cloud-topped boundary layers and the vertical positions of the cloud layers for all IFC 5 days in which soundings were launched. We stress that these rules were applied only to estimate the presence and locations of boundary layer clouds. Throughout IFC 5, mid- and high-level clouds were also present, but they are not considered in this study.

REFERENCES

Anthes, R. A., 1983: Regional models of the atmosphere in middle latitudes. *Mon. Wea. Rev.,* **111,** 1306–1335.

Atkinson, B. W., 1981: *Mesoscale Atmospheric Circulations.* Academic Press, 495 pp.

Betts, A. K., J. H. Ball, and A. C. M. Beljaars, 1993: Comparison between the land surface response of the ECMWF model and the FIFE-1987 data. *Quart. J. Roy. Meteor. Soc.*, **119,** 975–1001.

Brutsaert, W., and M. Sugita, 1990: The extent of the unstable Monin–Obukhov layer for temperature and humidity above complex hilly grassland. *Bound.-Layer Meteor.,* **51,** 383–400.

——, and ——, 1992: Application of self-preservation in the diurnal evolution of the surface energy budget to determine daily evaporation. *J. Geophys. Res.,* **97,** 18 377–18 382.

——, ——, and L. J. Fritschen, 1990: Inner region humidity characteristics of the neutral boundary layer over Prairie terrain. *Water Resour. Res.,* **26,** 2931–2936.

Bunker, A. F., 1953: On the determination of moisture gradients from radiosonde records. *Bull. Amer. Meteor. Soc.,* **34,** 406–409.

Chen, F., and R. Avissar, 1994: The impact of land–surface wetness heterogeneity on mesoscale heat fluxes. *J. Appl. Meteor.,* **33,** 1323–1340.

Connell, B. H., and D. R. Miller, 1995: An interpretation of radiosonde errors in the atmospheric boundary layer. *J. Appl. Meteor.,* **34,** 1070–1081.

Dastoor, A., and T. N. Krishnamurti, 1991: The landfall and structure of tropical cyclones: The sensitivity of model prediction to soil and moisture parameterization. *Bound.-Layer Meteor.,* **55,** 345–380.

Desjardins, R. L., P. H. Schuepp, J. I. MacPherson, and D. J. Buckley, 1992: Spatial and temporal variations of the fluxes of carbon dioxide and sensible and latent heat over the FIFE site. *J. Geophys. Res.,* **97,** 18 467–18 476.

Dickinson, R. E., 1989: Modeling the effects of Amazonian deforestation on a regional surface climate: A review. *Agric. For. Meteor.,* **47,** 339–348.

——, 1993: Changes in land use. *Climate System Modeling,* K. E. Trenberth, Ed., Cambridge University Press, 689–701.

Djuric, D., 1994: *Weather Analysis.* Prentice-Hall, 304 pp.

Golden, J. H., R. Serafin, V. Lally, and J. Facundo, 1986: Atmospheric sounding system. *Mesoscale Meteorology and Forecasting,* P. Ray, Ed., Amer. Meteor. Soc., 50–70.

Goutorbe, J.-P., and Coauthors, 1993: HAPEX-Sahel: A large scale study of land–atmosphere interactions in the semi-arid Tropics. *Ann. Geophys.,* **12,** 53–64.

Gravel, S., and A. Staniforth, 1992: Variable resolution and robustness. *Mon. Wea. Rev.,* **120,** 2633–2640.

Kanemasu, E. T., and Coauthors, 1992: Surface flux measurements in FIFE: An overview. *J. Geophys. Res.,* **97,** 18 547–18 556.

Kuo, H.-C., and W. H. Schubert, 1988: Stability of cloud-topped boundary layer. *Quart. J. Roy. Meteor. Soc.,* **114,** 915–944.

Luers, J. K., and R. E. Eskridge, 1995: Temperature corrections for the VIZ and Vaisala radiosondes. *J. Appl. Meteor.,* **34,** 1241–1253.

Lynn, B. H., D. Rind, and R. Avissar, 1995: The importance of mesoscale circulations generated by subgrid-scale landscape heterogeneities. *J. Climate,* **8,** 191–205.

Noilhan, J., and P. LaCarrére, 1995: GCM grid-scale evaporation from mesoscale modeling. *J. Climate,* **8,** 206–223.

Prince, S. D., and Coauthors, 1995: The Hydrological Atmospheric Pilot Experiment in the Sahel (HAPEX-Sahel). *Remote Sens. Environ.,* **51,** 215–234.

Sellers, P. J., and J. L. Dorman, 1987: Testing the simple biosphere model (SiB) using point micrometeorological and biophysical data. *J. Climate Appl. Meteor.,* **26,** 622–651.

——, F. G. Hall, G. Asrar, D. E. Strebel, and R. E. Murphy, 1988: The First ISLSCP Field Experiment (FIFE). *Bull. Amer. Meteor. Soc.*, **69,** 22–27.

——, ——, ——, ——, and ——, 1992: An overview of the First International Satellite Land Surface Climtatology Project (ISLSCP) Field Experiment (FIFE). *J. Geophys. Res.*, **97,** 18 345–18 371.

Siems, S. S., C. S. Bretherton, M. B. S. Shy, and R. E. Breidenthal, 1990: Buoyancy reversal and cloud-top entrainment instability. *Quart. J. Roy. Meteor. Soc.*, **116,** 705–739.

Smith, E. A., M. M.-K. Wai, H. J. Cooper, M. T. Rubes, and A. Hsu, 1994: Linking boundary layer circulations and surface processes during FIFE 89. Part I: Observational analysis. *J. Atmos. Sci.*, **51,** 1497–1529.

Stull, R. B., 1988: *An Introduction to Boundary Layer Meteorology*. Kluwer Academic, 666 pp.

Sugita, M., and W. Brutsaert, 1990: Wind velocity measurements in the neutral boundary layer above hilly prairie. *J. Geophys. Res.*, **95,** 7617–7624.

Sun, J., and L. Mahrt, 1994: Spatial distribution of surface fluxes estimated from remotely sensed variable. *J. Appl. Meteor.*, **33,** 1341–1353.

Wai, M. M.-K., 1992: Persistence of marine boundary clouds in a case with inhomogeneous surface forcing. *Beitr. Phys. Atmos.*, **64,** 335–338.

Wallace, J. S., 1994: Hydrological processes and dryland degradation. *Bull. World Meteor. Org.*, **43,** 22–28.

WMO, 1983: Guide to meteorological instruments and methods of observation. WMO Publication No. 8, 5th ed., ISBN# 92–63–1500F–4, Secretariat of WMO, 13.1–13.26. [Available from World Meteor. Org., Case Postale 2300, CH-1211 Geneva 2, Switzerland.]

Zeng, X., and R. A. Pielke, 1995: Landscape-induced atmospheric flow and its parameterization in large-scale numerical models. *J. Climate*, **8,** 1156–1177.